

Self-consistent calculation of Compton profiles, x-ray structure factors, and band structure for diamond

R. Heaton and E. Lafon

Department of Physics, Oklahoma State University, Stillwater, Oklahoma 74074

(Received 10 August 1977)

A self-consistent calculation of the band structure of diamond has been performed using the method of linear combination of atomic orbitals with a wave-vector-dependent optimized orbital basis set. Nineteen points in (1/48)th of the Brillouin zone were used to determine the charge density in each of the 11 iterations needed to reach self-consistency. The resultant self-consistent band states are then used to predict such ground-state properties as Compton profiles and x-ray structure factors.

I. INTRODUCTION

Among the group-IV materials, diamond occupies a unique position from the theoretical standpoint due to the fact that the covalent bonds are well defined.¹ Since the covalent-bond model plays an important role in the understanding of silicon² and the other group-IV materials, diamond is a frequent candidate for theoretical investigations.³ Additionally, diamond has an unusually small core with two-thirds of its electrons participating in valence states. This small core is of advantage not only in reducing the overall computational complexity but is also advantageous from the experimental point of view in that such a small core does not tend to dominate such ground-state property measurements as Compton profile and x-ray structure factors.

This paper presents a self-consistent Hartree-Fock-Slater calculation for diamond using the method of linear combination of atomic orbitals (LCAO).^{4,5} The method of LCAO has now been successfully applied, self-consistently, within the Hartree-Fock-Slater formalism to both metals⁶ and insulators.⁷ In addition, the method of LCAO has recently been employed in a self-consistent Hartree-Fock calculation of diamond.⁸ In performing these calculations self-consistently and in evaluating associated bulk properties, the extent of variational freedom permitted must usually be balanced against the need to economically evaluate the band states at a large number of low-symmetry points within the Brillouin zone. The LCAO calculation presented here introduces a generalization of the concept of optimized orbitals² which provides a high degree of variational freedom while maintaining a manageable secular equation for rapid evaluations of the band states throughout the Brillouin zone. This generalized optimized orbital approach is then extended into a self-consistent framework and applied to diamond with specific emphasis on the valence-band structure and

such associated ground properties as Compton profile and x-ray structure factors.

II. DIAMOND SYMMETRY

The diamond structure can be viewed as the superposition of two face-centered-cubic (fcc) arrays of carbon atoms each having the same lattice constant a_0 chosen here to be 6.728 a.u. The edges of the face-centered cubes for these two arrays are parallel but displaced from one another by $\frac{1}{4}a_0\sqrt{3}$ along the cube main diagonal. In this calculation, the origin is placed at the center of inversion which is located on this main diagonal at a point midway between the atoms of these two interpenetrating sublattices and with coordinate axes parallel to the cube edges. With this choice of coordinates, the positions of the carbon atoms are given by

$$\vec{T}_{\nu i} = \vec{R}_{\nu} + \vec{t}_i, \quad i = 1, 2, \quad (1)$$

where

$$\vec{t}_1 = -\frac{1}{8}a_0(1, 1, 1) = -\vec{t}_2,$$

$$\vec{R}_{\nu} = \nu_1\vec{a}_1 + \nu_2\vec{a}_2 + \nu_3\vec{a}_3,$$

and where ν_1, ν_2, ν_3 are integers and the primitive lattice vectors $\vec{a}_1, \vec{a}_2, \vec{a}_3$ are given by

$$\vec{a}_1 = \frac{1}{2}a_0(1, -1, 0),$$

$$\vec{a}_2 = \frac{1}{2}a_0(0, 1, -1), \quad (2)$$

$$\vec{a}_3 = a_0(0, 0, 1).$$

The volume of the Wigner-Seitz cell centered at the origin is designated by Ω , has the value $\frac{1}{4}a_0^3$ for its magnitude, and contains two atoms located at positions \vec{t}_1 and \vec{t}_2 .

The reciprocal lattice for this periodic structure is body-centered cubic (bcc) with lattice vectors \vec{K}_{ν} given by

$$\vec{K}_{\nu} = \nu_1\vec{b}_1 + \nu_2\vec{b}_2 + \nu_3\vec{b}_3, \quad (3)$$

where

$$\begin{aligned}\vec{b}_1 &= 2\pi(2, 0, 0)/a_0, \\ \vec{b}_2 &= 2\pi(2, 2, 0)/a_0, \\ \vec{b}_3 &= 2\pi(1, 1, 1)/a_0.\end{aligned}\quad (4)$$

The Brillouin zone associated with this lattice is designated by Ω_k and has the value $(2\pi)^3/\Omega$ for its magnitude.

In addition to translational symmetry, the diamond structure has rotation-reflection symmetry which, when adjoined with translation, produces a nonsymmorphic space group with point group O_h . As a consequence of this rotational symmetry, the wave functions and eigenvalues associated with any point in the Brillouin zone can be obtained directly from knowledge of the wave functions and eigenvalues of that portion of the Brillouin zone called the irreducible wedge (IW). A segment of the Brillouin zone is said to constitute an irreducible wedge if its volume is $\Omega_k/48$ and if the segment generates the entire Brillouin zone under the application of the 48 operations of O_h . The irreducible wedge chosen here consists of all points

$$\vec{k} = \kappa_1 \vec{b}_1 + \kappa_2 \vec{b}_2 + \kappa_3 \vec{b}_3,$$

which lie within the Brillouin zone and for which κ_1 , κ_2 , and κ_3 are all greater than or equal to zero.

In an analogous manner, an irreducible volume (IV) of the Wigner-Seitz cell with volume $\frac{1}{48}\Omega$ can be constructed such that any band-state wave function can be constructed throughout the entire crystal from knowledge of the behavior of the wave functions within the irreducible volume.

Substantial use is made of both the irreducible wedge and irreducible volume in order to eliminate redundant computations.

III. BAND-STATE HAMILTONIAN

The energy of the n th band at point \vec{k} in the Brillouin zone $E_n(\vec{k})$ and the associated wave functions with degeneracy label i , $\psi_{n,i}(\vec{k}, \vec{r})$, are obtained by solving the equation

$$[-\frac{1}{2}\nabla^2 + V(\vec{r})]\psi_{n,i}(\vec{k}, \vec{r}) = E_n(\vec{k})\psi_{n,i}(\vec{k}, \vec{r}), \quad (5)$$

for all points of interest in the Brillouin zone. In the above expression, $V(\vec{r})$ is the effective Hartree-Fock-Slater potential⁹ and is invariant under the diamond space group. The potential $V(\vec{r})$ can be expressed as a simple sum of a Coulomb term $V_{\text{Coul}}(\vec{r})$ and an effective "exchange" $V_{\text{ex}}(\vec{r})$ as

$$V(\vec{r}) = V_{\text{Coul}}(\vec{r}) + V_{\text{ex}}(\vec{r}), \quad (6)$$

where $V_{\text{Coul}}(\vec{r})$ and $V_{\text{ex}}(\vec{r})$ are expressible in terms of the absolute value of the electronic charge density $\rho(\vec{r})$ and the atomic number of carbon Z_C as

$$\nabla^2 V_{\text{Coul}}(\vec{r}) = 4\pi Z_C \sum_{\nu} \sum_{\tau} \delta(\vec{r} - \vec{T}_{\nu\tau}) - 4\pi\rho(\vec{r}), \quad (7)$$

$$V_{\text{ex}}(\vec{r}) = -\frac{3}{2}(3/\pi)^{1/3}\rho^{1/3}(\vec{r}), \quad (8)$$

where $\rho^{1/3}(\vec{r})$ is the positive cube root of the absolute value of the electronic charge density evaluated at \vec{r} .

Since the LCAO method as used here deals exclusively with the Fourier coefficients of the crystal potential, it is convenient to reexpress $V(\vec{r})$ and $\rho(\vec{r})$ as

$$V(\vec{r}) = \sum_{\nu} [V_{\text{Coul}}(\vec{K}_{\nu}) + V_{\text{ex}}(\vec{K}_{\nu})] \cos \vec{K}_{\nu} \cdot \vec{r}, \quad (9)$$

$$\rho(\vec{r}) = \sum_{\nu} \rho(\vec{K}_{\nu}) \cos \vec{K}_{\nu} \cdot \vec{r}, \quad (10)$$

where use has been made of the inversion symmetry at $\vec{r}=0$. The Fourier coefficients for potential are given by

$$V_{\text{Coul}}(\vec{K}_{\nu}) = \frac{1}{N\Omega} \int_{N\Omega} V_{\text{Coul}}(\vec{r}) \cos \vec{K}_{\nu} \cdot \vec{r} d\tau, \quad (11)$$

$$V_{\text{ex}}(\vec{K}_{\nu}) = \frac{1}{N\Omega} \int_{N\Omega} V_{\text{ex}}(\vec{r}) \cos \vec{K}_{\nu} \cdot \vec{r} d\tau, \quad (12)$$

where N represents, symbolically, the number of unit cells of the crystal. These coefficients of potential can be related directly to charge density by use of Eqs. (7) and (8), yielding

$$K_{\nu}^2 V_{\text{Coul}} = -4\pi[(2Z_C/\Omega) \cos \vec{K}_{\nu} \cdot \vec{t}_1 - \rho(\vec{K}_{\nu})], \quad (13)$$

$$V_{\text{ex}}(\vec{K}_{\nu}) = -\frac{3}{2}(3/\pi)^{1/3}\rho^{1/3}(\vec{K}_{\nu}), \quad (14)$$

where $\rho(\vec{K}_{\nu})$ and $\rho^{1/3}(\vec{K}_{\nu})$ are the Fourier coefficients of $\rho(\vec{r})$ and $\rho^{1/3}(\vec{r})$, respectively. Thus the $V(\vec{K}_{\nu})$ needed to produce the band structure and associated bulk properties can be obtained directly from knowledge of charge density.

IV. LCAO BAND CALCULATION FOR DIAMOND

The LCAO approach to crystalline materials as utilized here is basically an application of the method of linear variation of parameters, where the individual members of the basis set are so constructed as to satisfy the Bloch condition. Two types of basis sets are used in this calculation and are designated as basis set I and basis set II. Basis set I consists entirely of single Gaussian Bloch sums b_{α}^{Λ} and contains 112 members. Basis set II consists of 18 Bloch sums each of which is a carefully selected linear combination of Gaussians from basis set I (contracted Gaussian orbitals). The procedure used for selecting this contracted set will be discussed further in Sec. V. For the present we will confine our development to basis set I since the contracted orbitals are simply a projection of the more general single Gaussian orbital basis.

The single Gaussian Bloch sums are of the form

$$b_{\alpha j}^{\Delta}(\vec{k}, \vec{r}) = N^{-1/2} I_{\alpha}^{\Delta} \times \sum_{\nu} e^{i\vec{k} \cdot \vec{R}_{\nu}} \bar{\chi}_{\alpha}^{\Delta}(\beta_j, \vec{r} - \vec{R}_{\nu}), \quad (15)$$

where

$$\alpha = s, p_x, p_y, p_z,$$

$$\Delta = +1, -1,$$

$$I_{\alpha}^{\pm} = -iI_{\alpha}^{\mp} = \begin{cases} 1 & \text{for } \alpha = s, \\ i & \text{for } \alpha = p_x, p_y, p_z, \end{cases}$$

and where $\bar{\chi}_{\alpha}^{\Delta}(\beta, \vec{r})$ is a linear superposition of Gaussian orbitals centered at \vec{t}_1 and \vec{t}_2 given by

$$\bar{\chi}_{\alpha}^{\Delta}(\beta, \vec{r}) = \chi_{\alpha}(\beta, \vec{r} - \vec{t}_1) + \Delta \chi_{\alpha}(\beta, \vec{r} - \vec{t}_2). \quad (16)$$

The Gaussian orbitals $\chi_{\alpha}(\beta, \vec{r})$ have orbital exponent β and are given by

$$\chi_s(\beta, \vec{r}) = e^{-\beta r^2}, \quad (17)$$

$$\chi_{p_x}(\beta, \vec{r}) = x e^{-\beta r^2},$$

etc. The set of β used in this calculation are the 14 exponents 4232.61, 634.882, 146.097, 42.4974, 18.1557, 14.1892, 5.14773, 3.9864, 1.96655, 1.14293, 0.49624, 0.35945, 0.15331, and 0.1146 obtained by Huizinga¹⁰ for the free carbon atom. Since the Bloch sums formed from atomic orbitals produce reasonable band structures,¹¹ such a single Gaussian expansion should adequately allow for the relaxation of these "tight-binding" orbitals in the crystalline environment. However, these new orbitals will now vary both with the band index n and the point \vec{k} within the Brillouin zone. This matter will be discussed further in Sec. V in connection with the choice of the contracted orbitals for basis set II. Using the Bloch basis $b_{\alpha j}^{\Delta}(\vec{k}, \vec{r})$, the wave functions $\psi_{n,i}(\vec{k}, \vec{r})$ and associated band energies $E_n(\vec{k})$ for the i th degeneracy of the n th band at point \vec{k} in the Brillouin zone are obtained from solutions of the matrix equation

$$[H(\vec{k}) - E_n(\vec{k})S(\vec{k})]\vec{a}(n, i|\vec{k}) = 0, \quad (18)$$

and the orthonormality condition

$$\int_{N\Omega} \psi_{n,i}^*(\vec{k}, \vec{r}) \psi_{n,i'}(\vec{k}, \vec{r}) d\tau = \delta_{nn'} \delta_{ii'}, \quad (19)$$

where the $\psi_{n,i}(\vec{k}, \vec{r})$ are given in terms of the components of the column matrix $\vec{a}(n, i|\vec{k})$ by

$$\psi_{n,i}(\vec{k}, \vec{r}) = \sum_{\alpha} \sum_{\Delta} \sum_j a_{\alpha j}^{\Delta}(n, i|\vec{k}) b_{\alpha j}^{\Delta}(\vec{k}, \vec{r}). \quad (20)$$

As a result of the choice of basis $b_{\alpha j}^{\Delta}(\vec{k}, \vec{r})$ given in Eq. (15), and the presence of inversion symmetry at the origin, the components of matrices $H(\vec{k})$ and $S(\vec{k})$ are real and are given by

$$H_{\alpha j; \alpha' j'}^{\Delta \Delta'}(\vec{k}) = \int_{N\Omega} b_{\alpha j}^{\Delta}(\vec{k}, \vec{r}) [-\frac{1}{2} \nabla^2 + V(\vec{r})] \times b_{\alpha' j'}^{\Delta'}(\vec{k}, \vec{r}) d\tau, \quad (21)$$

$$S_{\alpha j; \alpha' j'}^{\Delta \Delta'}(\vec{k}) = \int_{N\Omega} b_{\alpha j}^{\Delta}(\vec{k}, \vec{r}) b_{\alpha' j'}^{\Delta'}(\vec{k}, \vec{r}) d\tau.$$

Due to the rotational symmetry mentioned earlier, if R_{γ} is a member of O_h and $\vec{\tau}_{\gamma}$ is the non-symmorphic translation associated with R_{γ} such that

$$V(R_{\gamma} \vec{r} + \vec{\tau}_{\gamma}) = V(\vec{r}), \quad (22)$$

$$\rho(R_{\gamma} \vec{r} + \vec{\tau}_{\gamma}) = \rho(\vec{r}), \quad (23)$$

then, from symmetry considerations,

$$E_n(R_{\gamma} \vec{k}) = E_n(\vec{k}), \quad (24)$$

$$\psi_{n,i}(R_{\gamma} \vec{k}, R_{\gamma} \vec{r} + \vec{\tau}_{\gamma}) = \sum_j C_{ij}^n(\gamma, \vec{k}) \psi_{n,j}(\vec{k}, \vec{r}), \quad (25)$$

and the eigenvectors $\vec{a}(n, i|R_{\gamma} \vec{k})$ at points outside the irreducible wedge are related to the $\vec{a}(n, i|\vec{k})$ within the irreducible wedge by

$$\vec{a}(n, i|R_{\gamma} \vec{k}) = U(\gamma, \vec{k}) \vec{a}(n, i|\vec{k}), \quad (26)$$

where the matrices $U(\gamma, \vec{k})$ and $C^n(\gamma, \vec{k})$ are unitary.

The relationships given in Eqs. (23), (25), and (26) greatly simplify the computation of bulk properties such as x-ray structure factors and Compton profile since they permit the required integrals over the Brillouin zone to be folded back into the irreducible wedge.

V. SELF-CONSISTENT LCAO

The self-consistent procedure is initiated by an initial guess, zeroth iteration, of the absolute value of the electronic charge density $\rho^0(\vec{r})$, where the integer superscript labels the iteration. In this calculation, the initial guess for $\rho^0(\vec{r})$ was chosen to be that produced by associating free-atom electronic charge densities $\rho_{\text{atom}}(\vec{r})$, with each atomic site of the diamond lattice. This yields the analytic expression

$$\rho^0(\vec{r}) = \sum_{\nu} \sum_{\vec{t}} \rho_{\text{atom}}(\vec{r} - \vec{T}_{\nu i}), \quad (27)$$

with Fourier coefficients given by

$$\rho^0(\vec{k}_{\nu}) = \frac{8\pi}{\Omega} \cos \vec{k}_{\nu} \cdot \vec{t}_1 \times \int_0^{\infty} \rho_{\text{atom}}(r) j_0(K_{\nu} r) r^2 dr. \quad (28)$$

The zeroth-iteration crystal potential $V^0(\vec{k}_{\nu})$ can then be obtained directly from Eqs. (13) and (14). The numerical procedure for evaluating $\rho^{1/3}(\vec{k}_{\nu})$ will be discussed in Sec. VI. Solution of Eq. (18)

for the zeroth-order band states $\psi_{n,i}^0(\vec{k}, \vec{r})$ yields a first iteration charge density $\rho^1(\vec{r})$, which can then be employed, as discussed in Sec. III, to create $V^1(\vec{k}_\nu)$, $\psi_{n,i}^1(\vec{k}, \vec{r})$, and so produce a second iteration charge density $\rho^2(\vec{r})$. This process is continued, using an iteration-averaging stabilizing technique¹² for the first few iterations, until the $\rho(\vec{k}_\nu)$ have stabilized to at least three significant figures.

Each iteration involves the evaluation of charge density and this in turn entails a numerical integration over 912 uniformly spaced mesh points within the Brillouin zone (19 points in the irreducible wedge). Since these points are, for the most part, without symmetry, solution of Eq. (18) involves a 112×112 secular equation. In addition to the difficulties normally associated with such large secular equations, the problem is further exacerbated by the fact that the overlap matrix elements formed from one or more of these single Gaussian Bloch sums can to a high degree of accuracy be expressed as a linear combination of the overlap matrix elements of the remaining Bloch sums. In order to remove these difficulties, the overlap matrix associated with each point \vec{k} in the Brillouin zone must be examined and the redundant Bloch sums removed from the secular equation. Although a high degree of variational freedom is desired, it has been found² that considerable accuracy can be obtained more economically using a small basis set of contracted Gaussian orbitals called optimized orbitals. Obviously, the accuracy obtained with this projected basis set is highly sensitive to the method by which the contracted orbitals are chosen. The procedure employed here for selecting this contracted set is based upon solution of the general single Gaussian problem [Eq. (18)] at points of high symmetry in the Brillouin zone. This technique is best presented by first using Eqs. (15) and (16) to rewrite Eq. (20) as

$$\psi_{n,i}(\vec{k}, \vec{r}) = N^{-1/2} \sum_{\nu} e^{i\vec{k} \cdot \vec{r}_\nu} \sum_{\alpha} \sum_{\Delta} I_{\alpha}^{\Delta} \bar{\phi}_{\alpha}^{\Delta}(n, i | \vec{k}, \vec{r}), \quad (29)$$

where

$$\begin{aligned} \bar{\phi}_{\alpha}^{\Delta}(n, i | \vec{k}, \vec{r}) &= \phi_{\alpha\Delta}(n, i | \vec{k}, \vec{r} - \vec{r}_1) \\ &+ \Delta \phi_{\alpha\Delta}(n, i | \vec{k}, \vec{r} - \vec{r}_2), \end{aligned}$$

and where the $\phi_{\alpha\Delta}(n, i | \vec{k}, \vec{r})$ are contractions of the original single Gaussians given by

$$\phi_{\alpha\Delta}(n, i | \vec{k}, \vec{r}) = \sum_j a_{\alpha j}^{\Delta}(n, i | \vec{k}) \chi_{\alpha}(\beta_j, \vec{r}). \quad (30)$$

The $\phi_{\alpha\Delta}(n, i | \vec{k}, \vec{r})$ are called optimized orbitals² and

are found to be sensitive to the energy $E_n(\vec{k})$ of the state $\psi_{n,i}(\vec{k}, \vec{r})$ in which they participate. For example $\phi_{p_x-}(4, 1 | \Gamma, \vec{r})$ and $\phi_{p_x+}(5, 1 | \Gamma, \vec{r})$ which participate in the top of the valence band and the bottom of the conduction band, respectively, differ only slightly from one another with the lower-energy orbital being slightly more localized or "tightly bound" than the higher-energy optimized orbital of the conduction band. The variation with energy of the self-consistent optimized p orbitals within the valence band is shown in Fig. 1 and clearly shows a trend toward greater localization with decreasing energy. As a general rule we find that the s -type and p -type optimized orbitals of the valence band tend to become more localized (tightly bound) as the energy decreases.

Since in a self-consistent calculation the occupied orbitals are of primary interest, we choose our contracted set to be optimized orbitals from the bottom, middle, and top of the valence-band energy range. In particular, the contracted set for the λ th iteration is

$$\begin{aligned} \phi_1^{\lambda}(\vec{r}) &= \phi_{s+}^{\lambda}(1, 1 | \Gamma, \vec{r}) \quad (\text{core state at } \Gamma), \\ \phi_2^{\lambda}(\vec{r}) &= \phi_{s+}^{\lambda}(3, 1 | \Gamma, \vec{r}) \\ &\quad (\text{bottom of valence band at } \Gamma), \\ \phi_3^{\lambda}(\vec{r}) &= \phi_{s+}^{\lambda}(2, 1 | X, \vec{r}) \\ &\quad (\text{bottom of valence band at } X), \\ \phi_4^{\lambda}(\vec{r}) &= \phi_{p_x-}^{\lambda}(2, 1 | X, \vec{r}) \\ &\quad (\text{bottom of valence band at } X), \\ \phi_5^{\lambda}(\vec{r}) &= \phi_{p_x-}^{\lambda}(4, 1 | \Gamma, \vec{r}) \\ &\quad (\text{top of valence band at } \Gamma), \\ \phi_6^{\lambda}(\vec{r}) &= y\phi_4^{\lambda}(\vec{r})/x, \quad \phi_7^{\lambda}(\vec{r}) = y\phi_5^{\lambda}(\vec{r})/x, \\ \phi_8^{\lambda}(\vec{r}) &= z\phi_4^{\lambda}(\vec{r})/x, \quad \phi_9^{\lambda}(\vec{r}) = z\phi_5^{\lambda}(\vec{r})/x. \quad (31) \end{aligned}$$

It is important to note that although only nine distinct orbitals are used in constructing the charge density for each iteration, these orbitals are reoptimized directly from the original single Gaussian set at each step in the iterative procedure. This has the effect of allowing the contracted basis to relax to the new potential $V^{\lambda}(\vec{r})$ of each successive iteration. An illustrative example of how these $\phi_j^{\lambda}(\vec{r})$ change from iteration to iteration is presented in Fig. 2, where the converged and first iteration values of ϕ_5 are presented along with the free atom $2p_x$ orbital. The results given in Fig. 2 indicate the importance of allowing the contracted basis to change from iteration to iteration and the inadequacy of a simple atomic-orbital basis set to reflect the relaxation of the atom

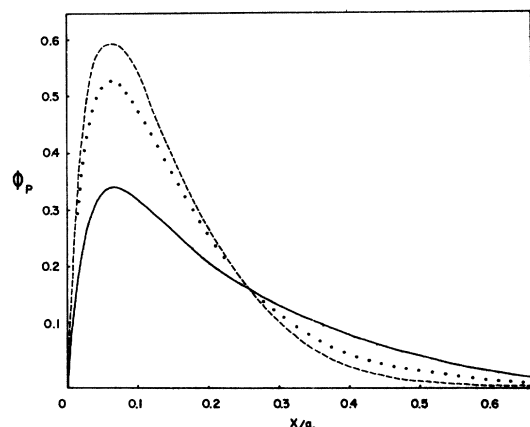


FIG. 1. Variation of self-consistent optimized p orbitals with energy. The dashed curve is the orbital from bottom of valence band at X point, the dotted curve is the orbital from top of the valence band at X point, and the solid curve is the orbital from top of valence band at Γ point.

in the crystalline environment.

Using the above set of contracted Gaussian orbitals $\phi_i^\lambda(\vec{r})$ the variational wave function for the λ th iteration is given by

$$\psi_{n,i}^\lambda(\vec{k}, \vec{r}) = \sum_j \sum_{\Delta} A_j^{\lambda\Delta}(n, i|\vec{k}) B_j^{\lambda\Delta}(\vec{k}, \vec{r}) \quad (32)$$

$$= N^{-1/2} \sum_{\nu} e^{i\vec{k} \cdot \vec{R}_{\nu}} \xi_{n,i}^{\lambda}(\vec{k}, \vec{r} - \vec{R}_{\nu}), \quad (33)$$

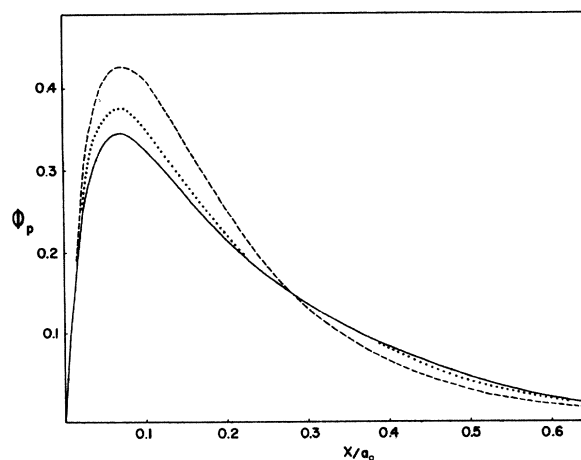


FIG. 2. Illustration of relaxation of optimized orbitals to the crystalline potential. The dashed curve is the atomic $2p$ orbital, the dotted (solid) curve is the p orbital from top of valence band at Γ point as obtained during the first (last) iteration.

where

$$B_j^{\lambda\Delta}(\vec{k}, \vec{r}) = N^{-1/2} I_j^{\Delta} \sum_{\nu} e^{i\vec{k} \cdot \vec{R}_{\nu}} [\phi_j^{\lambda}(\vec{r} - \vec{R}_{\nu} - \vec{t}_1) + \Delta \phi_j^{\lambda}(\vec{r} - \vec{R}_{\nu} - \vec{t}_2)], \quad (34)$$

and where the $A_j^{\lambda\Delta}$ are the 18 variational coefficients obtained by solving the appropriate secular equation.

The self-consistent band structure for diamond is presented in Fig. 3. Since we are interested here in the conduction band as well as the valence band, additional variational freedom was provided by including optimized X -point orbitals at the bottom of the conduction band. Since, as discussed earlier, ϕ_5 , ϕ_7 , and ϕ_9 are essentially optimized orbitals for the bottom of the conduction band at Γ , the band structure for the lower portion of the conduction band should be fairly accurate. This calculation predicts an indirect band gap of 5.2 eV in excellent agreement with the experimental value¹³ of 5.4 eV. The associated minimum of the conduction band is calculated to lie at $2\pi(0.68, 0, 0)/a_0$ as compared with an experimental value¹⁴ of $2\pi(0.75, 0, 0)/a_0$. The Hartree-Fock indirect band gap, on the other hand, has been found to be 13.7 eV.⁸ This lack of agreement between Hartree-Fock and experiment is attributed to correlation. For the remainder of this paper, comparison with Hartree-Fock will be restricted to ground-state properties where correlation plays a lesser role and agreement between Hartree-Fock and experiment is substantially better. The width of the valence band as calculated here is 21.1 eV which, while in excellent agreement with the experimental result of 21 eV reported by Gora *et al.*,¹⁵ is in substantial disagreement with the result of 24.2 eV reported by McFeely *et al.*¹⁶

VI. CALCULATION OF CHARGE DENSITY AND X-RAY STRUCTURE FACTORS

A. Evaluation of charge density in direct space

Using the notation previously developed, the absolute value of electronic charge density for the λ th iteration $\rho^\lambda(\vec{r})$ can be expressed as an integration over the Brillouin zone of the form

$$\rho^\lambda(\vec{r}) = \frac{2N}{\Omega_R} \int_{\Omega_k} \sum_{n,j} \psi_{n,j}^{\lambda*}(\vec{k}, \vec{r}) \psi_{n,j}^\lambda(\vec{k}, \vec{r}) d^3k, \quad (35)$$

where the summations over n and j are over all occupied states at \vec{k} and the integration over the Brillouin zone is performed numerically by evaluating the integrand over the uniform mesh

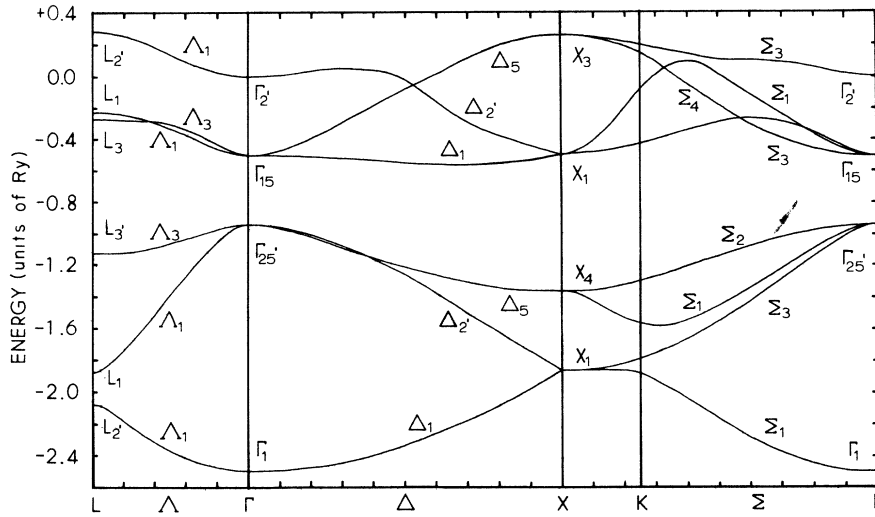


FIG. 3. Self-consistent band structure of diamond using optimized orbital basis.

$$\vec{k}_m = \frac{2m_1+1}{2N_1}\vec{I}_1 + \frac{2m_2+1}{2N_2}\vec{I}_2 + \frac{2m_3+1}{2N_3}\vec{I}_3. \quad (36)$$

In Eq. (36), the vectors \vec{I}_1 , \vec{I}_2 , and \vec{I}_3 are equal to $\frac{1}{2}\vec{b}_1$, $\frac{3}{8}\vec{b}_2$, and $\frac{1}{2}\vec{b}_3$, respectively, and form the edges of the irreducible wedge. Due to the symmetry relations of Eq. (25), the $\psi_{n,j}(\vec{k}_m, \vec{r})$ need only be calculated for those points \vec{k}_m which lie within the irreducible wedge.

B. Multipole fit of $\rho(\vec{r})$ and $\rho^{1/3}(\vec{r})$

A natural extension of Eq. (27) to the more complicated task of obtaining an analytic expression for $\rho^\lambda(\vec{r})$ of the λ th iteration is

$$\rho_{\text{fit}}^\lambda(\vec{r}) = \sum_{\nu} \sum_i f_i^\lambda(\vec{r} - \vec{T}_{\nu i}), \quad (37)$$

where $f_i^\lambda(\vec{r})$ is a parameterized analytic function with parameters so chosen that Eq. (37) constitutes an accurate least-squares fit to $\rho^\lambda(\vec{r})$. An analysis of the accuracy of this fitting procedure will be presented later in this section. The inversion symmetry of diamond is satisfied by the restriction

$$f_1^\lambda(\vec{r}) = f_2^\lambda(-\vec{r}). \quad (38)$$

The additional rotational symmetry implied by Eq. (23) would be automatically satisfied by requiring the $f_i^\lambda(\vec{r})$ to be spherically symmetric. However, such a restriction would produce a null value for the "forbidden" reflection $\vec{K}_o = 2\pi(2, 2, 2)/a_o$, while experiment measures a nonzero value for this reflection. Additionally, the fact that the experimental structure factors associated with different stars of the same magnitude are often reported as equal is simply due to the fact that the experiments

were performed on a powdered sample and do not imply that single-crystal measurements would predict equal structure factors. These points have been discussed in detail by Dawson.¹⁷ As a result of these considerations, the $f_i^\lambda(\vec{r})$ are not restricted to be spherically symmetric but rather are expanded in a multipole expansion of the form

$$f_1^\lambda(\vec{r}) = \sum_l g_l^\lambda(r) \sum_m C_l^m Y_l^m(\hat{r}), \quad (39)$$

where the summation on l is truncated after $l=4$. The tetrahedral site symmetry excludes $l=1$ and $l=2$ and allows only one combination for each of the terms $l=0, 3$, and 4 identified as monopole, octopole and hexadecapole, respectively. As a result of these symmetry restrictions, the fitting function is of the general form

$$f_1^\lambda(\vec{r}) = g_0^\lambda(r) + g_3^\lambda(r)(xyz/r^2) + g_4^\lambda(r) \times (x^4 + y^4 + z^4 - 3r^4/5)/r^3. \quad (40)$$

For the purposes of this calculation, the $g_l^\lambda(r)$ are chosen to be of the form

$$g_l^\lambda(r) = \sum_{i=1}^8 \sigma_{l,i}^\lambda r^{n_i} e^{-\mu_i r} + \delta_{l,0} \sum_{i=9}^{12} \sigma_{0,i}^\lambda r^{n_i} e^{-\mu_i r}, \quad (41)$$

where the sets $\{n_i\}$ and $\{\mu_i\}$ are $\{0, 1, 2, 3, 4, 5, 6, 7, 0, 0, 0, 0\}$ and $\{3, 3, 3, 3, 3, 3, 3, 3, 10, 20, 35, 100\}$, respectively. The linear coefficients $\sigma_{l,i}^\lambda$ are determined by a least-squares fit to $\rho^\lambda(\vec{r})$ as tabulated within the irreducible volume of the Wigner-Seitz cell. To evaluate the convergence of this multipole expansion, the self-consistent Fourier coefficients of the charge density obtained using only the $l=0$ term, $\rho_0(\vec{K}_\mu)$, both the $l=0$ and $l=3$ terms, $\rho_{0,3}(\vec{K}_\mu)$, and the $l=0, 3$, and 4 terms,

$\rho_{0,3,4}(\vec{K}_\mu)$ are presented in the second, third, and fourth columns of Table I. In this calculation, the tabulated $\rho(\vec{r})$ are obtained from Eq. (35) using a six-point numerical integration over the irreducible wedge. Examination of Table I shows satisfactory l convergence and also tends to indicate that the radial fitting functions $r^{nl}e^{-\mu r}$ are adequate.

For the evaluation of the $\rho^{1/3}(\vec{K}_\mu)$, a similar multipole expansion is used to fit the positive cube root of charge density as tabulated over the irreducible volume of the Wigner-Seitz cell.

C. Evaluation of ρ in reciprocal space

In order to further test the multipole convergence and, in addition, to test the validity of a six point integration over the irreducible wedge, an alternative procedure for evaluating the $\rho^\lambda(\vec{K}_\mu)$ without recourse to a multipole expansion was developed. In this procedure, the wave functions $\psi_{n,j}^\lambda(\vec{k}, \vec{r})$ for the λ th iteration are expressed in the form of Eq. (33). Using this expression and Eq. (25), the Fourier components of charge density, $\rho^\lambda(\vec{K}_\mu)$, can be shown to be

$$\rho^\lambda(\vec{K}_\mu) = \frac{2}{\Omega} \sum_n \sum_\gamma \int_{\text{IW}} Z_{n,\gamma}^\lambda(\vec{k}, \vec{K}_\mu) d^3k, \quad (42)$$

where n is summed over all occupied bands at point \vec{k} , the summation on γ is over all 48 operations R_γ of the cubic point group O_h , and the integral is over a single irreducible wedge. The integrand $Z_{n,\gamma}^\lambda(\vec{k}, \vec{K}_\mu)$ in Eq. (42) is given by

$$\begin{aligned} Z_{n,\gamma}^\lambda(\vec{k}, \vec{K}_\mu) = & \sum_\nu \sum_j e^{i(R_\gamma \vec{k}_\nu)_\nu \cdot \vec{\tau}_\gamma} \\ & \times \bar{\xi}_{n,j}^{\lambda*}(\vec{k}, \vec{k} - R_\gamma(\vec{k}_\nu + \vec{K}_\mu)) \\ & \times \bar{\xi}_{n,j}^\lambda(\vec{k}, \vec{k} - R_\gamma \vec{K}_\mu), \end{aligned} \quad (43)$$

where the $\bar{\xi}_{n,j}^\lambda(\vec{k}, \vec{k})$ are related to the $\xi_{n,j}^\lambda(\vec{k}, \vec{r})$ by

$$\bar{\xi}_{n,j}^\lambda(\vec{k}, \vec{k}) = (2\pi)^{-3/2} \int \xi_{n,j}^\lambda(\vec{k}, \vec{r}) e^{-i\vec{k} \cdot \vec{r}} d\tau, \quad (44)$$

and where the relationship between $\vec{\tau}_\gamma$ and R_γ is given by Eq. (23). As before, the integration over the irreducible wedge is performed numerically using the uniform mesh of Eq. (36). The $\rho(\vec{K}_\mu)$ which results from a six-point $[\rho(\vec{K}_\mu)]_6$ and a 19-point $[\rho(\vec{K}_\mu)]_{19}$ integration over the irreducible wedge are presented in the last two columns of Table I. Comparison of $[\rho(\vec{K}_\mu)]_6$ with the corresponding multipole expansion again supports the conclusions that truncation after $l=4$ is justified. Comparison between the six-point and the 19-point integration schemes shows that they agree well for all \vec{K}_μ and that the agreement improves with

TABLE I. Self-consistent Hartree-Fock-Slater Fourier coefficients of charge density for diamond; a comparison of various computational techniques.

| hkl | $\frac{1}{2}\Omega\rho_0$ | $\frac{1}{2}\Omega\rho_{0,3}$ | $\frac{1}{2}\Omega\rho_{0,3,4}$ | $\frac{1}{2}\Omega[\rho]_6^a$ | $\frac{1}{2}\Omega[\rho]_{19}$ |
|-------|---------------------------|-------------------------------|---------------------------------|-------------------------------|--------------------------------|
| 111 | -2.357 | -2.356 | -2.356 | -2.356 | -2.368 |
| 220 | -2.013 | -2.018 | -2.017 | -2.017 | -2.022 |
| 311 | -1.231 | -1.234 | -1.235 | -1.235 | -1.236 |
| 222 | 0.0 | 0.071 | 0.072 | 0.071 | 0.075 |
| 400 | -1.621 | -1.590 | -1.589 | -1.589 | -1.590 |
| 331 | 1.101 | 1.105 | 1.105 | 1.104 | 1.106 |
| 422 | 1.457 | 1.451 | 1.452 | 1.452 | 1.452 |
| 511 | 0.993 | 0.994 | 0.991 | 0.991 | 0.991 |
| 333 | 0.993 | 0.988 | 0.986 | 0.986 | 0.986 |

^a $[\rho]_6$ and $[\rho]_{19}$ correspond to 6-point and 19-point integrations, respectively, over the irreducible wedge.

increasing magnitude of \vec{K}_μ . The improved agreement with increasing K_μ is easily understood since at large K_μ the major contribution to $\rho^\lambda(\vec{K}_\mu)$ comes from the core states which, being tightly bound and relatively insensitive to the crystalline environment, produces an integrand which is essentially constant over the volume of the irreducible wedge. Although the errors introduced by a six-point quadrature are minor even at small \vec{K}_μ , the possibility of cumulative reinforcement with successive iteration is obviated by calculating the first nine $\rho^\lambda(\vec{K}_\mu)$ for each iteration directly from Eq. (42) using the 19-point quadrature. The remaining $\rho^\lambda(\vec{K}_\mu)$ are evaluated for each iteration using the multipole expansion and six-point integration over the irreducible wedge.

D. X-Ray structure factors

The self-consistent Hartree-Fock-Slater x-ray structure factors $F_{\text{HFS}}^{\text{SCF}}(\vec{K}_\mu)$ for the limit of rigid lattice are presented in the second column of Table II and are related to the Fourier coefficients of the self-consistent charge density $\rho(\vec{K}_\mu)$ presented in the last column of Table I by

$$F_{\text{HFS}}^{\text{SCF}}(\vec{K}_\mu) = 4\Omega\rho(\vec{K}_\mu). \quad (45)$$

The corresponding self-consistent Hartree-Fock structure factors $F_{\text{HF}}^{\text{SCF}}(\vec{K}_\mu)$ of Euwema⁸ are given in column 3. The experimental structure factors of Göttlicher and Wöfel corrected for the effects of isotropic thermal vibration are given in column 4. Comparison of column 2 with column 4 shows good agreement between the present theory and experiment with the exception of the 400 reflection which is in significant disagreement. Interestingly, the largest disagreement of experiment with the Hartree-Fock results of Euwema is again the 400

reflection. With the exception of this reflection, these two theoretical results are in substantially equivalent agreement with experiment. For quantitative comparison, it is useful to employ the agreement factor R defined in the usual way as

$$R = \sum |F_{\text{expt}} - F_{\text{theory}}| / \sum |F_{\text{expt}}|.$$

The agreement factors for Hartree-Fock-Slater and for Hartree-Fock are 3.4% and 2.7%, respectively.

In addition, the Hartree-Fock-Slater form factors are seen to be predominately larger in absolute magnitude than those of experiment. This observation is consistent with the suggestion by Dawson¹⁹ that the experimental results of Göttlicher and Wöfel must be multiplied by a scale factor somewhat larger than 1.007 in order to renormalize to absolute intensity. The scale factor which produces the best agreement between the present self-consistent Hartree-Fock-Slater form factors and those of experiment can be obtained by minimizing the agreement factor. The scale factor so obtained is determined to be 1.008 and is in excellent agreement with Dawson.

VII. COMPTON PROFILE

A. Computational procedure

In order to make a direct comparison of the experimental Compton profiles^{20,21} with the self-consistent Hartree-Fock-Slater results of this work, a method for calculating the theoretical Compton profiles using the impulse approximation²² has been developed and applied to diamond. Within the impulse approximation, the Compton profile $J(q, \hat{k})$ is related to the band states by the expression

$$J(q, \hat{k}) = \int \delta(q - \hat{k} \cdot \vec{\kappa}) \rho(\vec{\kappa}) d^3k, \quad (46)$$

where $\rho(\vec{\kappa})$ is the momentum density per atom given by

$$\rho(\vec{\kappa}) = \Omega_k^{-1} \int_{\Omega_k} \sum_n \sum_j \psi_{n,j}^*(\vec{k}, \vec{\kappa}) \psi_{n,j}(\vec{k}, \vec{\kappa}) d^3k, \quad (47)$$

and where the summations on n and j are over the six occupied band states at each point \vec{k} in the Brillouin zone. The $\psi_{n,j}(\vec{k}, \vec{\kappa})$ of Eq. (47) are the band states in the momentum representation and are related to the $\psi_{n,j}(\vec{k}, \vec{r})$ by

$$\psi_{n,j}(\vec{k}, \vec{\kappa}) = (2\pi)^{-3/2} \int \psi_{n,j}(\vec{k}, \vec{r}) e^{-i\vec{\kappa} \cdot \vec{r}} d\tau. \quad (48)$$

If the wave functions are written in the form of Eq. (33), then explicit use of the translational

TABLE II. X-ray structure factors for diamond.

| hkl | $F_{\text{HFS}}^{\text{SCF}}$ | $F_{\text{HF}}^{\text{SCF}^a}$ | F_{expt}^b |
|-------|-------------------------------|--------------------------------|---------------------|
| 111 | -18.945 | -18.657 | -18.787 |
| 220 | -16.181 | -15.445 | -15.778 |
| 311 | -9.886 | -9.456 | -9.405 |
| 222 | 0.601 | 0.689 | 1.206 ^c |
| 400 | -12.718 | -12.359 | -11.836 |
| 331 | 8.847 | 8.637 | 8.932 |
| 422 | 11.615 | 11.339 | 11.547 |
| 511 | 7.926 | | 8.023 |
| 333 | 7.884 | | 8.023 |

^aReference 8.

^bReference 18.

^cWeiss and Middleton in private communication to B. Dawson (Ref. 19).

symmetry of the Bloch sum reduces the expression for the momentum density, $\rho(\vec{\kappa})$, to the simple analytic expression

$$\rho(\vec{\kappa}) = \sum_n \sum_j |\tilde{\xi}_{n,j}(\vec{\kappa}, \vec{\kappa})|^2, \quad (49)$$

where the $\tilde{\xi}_{n,i}(\vec{\kappa}, \vec{\kappa})$ are given by Eq. (44) with the understanding that the $|\xi_{n,j}(\vec{\kappa}, \vec{\kappa})|^2$ are to be considered periodic in \vec{k} , i.e.,

$$|\xi_{n,j}(\vec{k} + \vec{K}_\mu, \vec{\kappa})|^2 = |\xi_{n,j}(\vec{k}, \vec{\kappa})|^2.$$

In the procedure adopted here for evaluating $J(q, \hat{k})$ from the theoretical band states, the integral over reciprocal space in Eq. (46) is reexpressed as a sum of integrals over the Brillouin zone having the form

$$J(q, \hat{k}) = \sum_\mu \int_{\Omega_k} \delta(q - \hat{k} \cdot (\vec{\kappa} + \vec{K}_\mu)) \times \rho(\vec{\kappa} + \vec{K}_\mu) d^3\kappa. \quad (50)$$

Using the symmetry relationship of Eq. (25), the expression for momentum density given in Eq. (47) yields the relation

$$\rho(R_\gamma \vec{\kappa}) = \rho(\vec{\kappa}) \quad (51)$$

for all operations R_γ of the point group O_h . Combining Eqs. (50) and (51) permits the Compton profile to be expressed as an integration over the irreducible wedge of the form

$$J(q, \hat{k}) = \sum_\mu \sum_\gamma \int_{\text{IW}} \delta(q - (R_\gamma \hat{k}) \cdot (\vec{\kappa} + \vec{K}_\mu)) \times \rho(\vec{\kappa} + \vec{K}_\mu) d^3\kappa. \quad (52)$$

The interpretation of Eq. (52) is that the Compton profile is expressed as a sum of integrals over a family of planes which intersect some portion of the irreducible wedge.

The evaluation of $J(q, \hat{k})$ from the band structure is facilitated by rewriting Eq. (52) as

$$J(q, \hat{k}) = \sum_{\mu} \sum_{\gamma} \bar{\rho}_{\mu}(q - (R_{\gamma} \hat{k}) \cdot \vec{K}_{\mu}, R_{\gamma} \hat{k}) \times A(q - (R_{\gamma} \hat{k}) \cdot \vec{K}_{\mu}, R_{\gamma} \hat{k}), \quad (53)$$

where $A(\lambda, \hat{n})$ is the area of the segment of the plane $\vec{k} \cdot \hat{n} = \lambda$ which lies within the irreducible wedge

$$A(\lambda, \hat{n}) = \int_{\text{IW}} \delta(\lambda - \vec{k} \cdot \hat{n}) d^3k, \quad (54)$$

and $\bar{\rho}_{\mu}(\lambda, \hat{n})$ is the average of $\rho(\vec{k} + \vec{K}_{\mu})$ over this same area segment. In evaluating the Compton profiles for diamond, the $A(\lambda, \hat{n})$ are evaluated analytically, while the $\bar{\rho}_{\mu}(\lambda, \hat{n})$ are evaluated numerically by first evaluating $\rho(\vec{k} + \vec{K}_{\mu})$ over the uniform mesh

$$\vec{k}'_m = (n_1 \vec{b}_1 + n_2 \vec{b}_2 + n_3 \vec{b}_3) / N, \quad (55)$$

where n_1, n_2, n_3 are integers so chosen that \vec{k}'_m lies within or upon the surface of the irreducible wedge and the integer N controls the density of points within the irreducible wedge. Using this numerical procedure, the Compton profiles for all five directions of \hat{k} and all values of q reported here can be obtained from a single evaluation of the $\rho(\vec{k}'_m + \vec{K}_{\mu})$ over the mesh \vec{k}'_m . The calculations of $J(q, \hat{k})$ for the five directions \hat{k} of the scattering vector were performed for different choices of the density parameter N . High-symmetry directions such as $\hat{k} = (1, 0, 0)$ were found to be suitably converged for N equal to ten due to the large separation between planes and the correspondingly high density of points per plane, while low-symmetry directions such as $\hat{k} = (2, 2, 1)/3$ were somewhat noisy for N equal to ten due to the lower density of points per plane. The final calculations were performed for an N value of 20 for which all five directions were found to be well converged.

B. Results and comparison with experiment and Hartree-Fock

The self-consistent Hartree-Fock-Slater Compton profile for $\hat{k} = (1, 0, 0)$ is presented in Fig. 4 by the solid line. Selected data points are indicated by filled circles. For comparison, the experimental measurements of Weiss and Phillips,²⁰ open circles, and the self-consistent Hartree-Fock calculations of Wepfer, Euwema, Surratt, and Wilhite,²³ triangles, are included in Fig. 4. In like manner, the Compton profiles for four lower symmetry directions are given in Fig. 5. The agreement of the present work with experiment is quite good. More surprising is the excel-

lent agreement between the present Hartree-Fock-Slater calculation and that of Hartree-Fock. Indeed, for all five directions of the scattering vector investigated, the agreement between Hartree-Fock and Hartree-Fock-Slater is even better than is the agreement of either theory with experiment with the Hartree-Fock-Slater results lying between those of Hartree-Fock and experiment.

Another definitive test of theory with experiment is to examine the anisotropies in the Compton profile associated with different scattering vector directions \hat{k} . These anisotropies have been measured and reported in graphical form by Reed and Eisenberger.²¹ These experimental results are reproduced approximately in Fig. 6 by open circles connected by straight lines. The reader is referred to the original paper for a more accurate presentation of the experimental anisotropies. The self-consistent Hartree-Fock-Slater results are given in Fig. 6 by the filled circles and the self-consistent Hartree-Fock results of Ref. (23) are presented as triangles. Considering the fact that the observed anisotropies are more than an order of magnitude smaller than the individual Compton profiles, the overall agreement between theory and experiment is quite good. Again, as with the Compton profiles themselves, the agreement between the present theory and that of Hartree-Fock is exceptional.

VIII. SUMMARY AND CONCLUSION

In this paper we have presented a method for obtaining an accurate self-consistent Hartree-

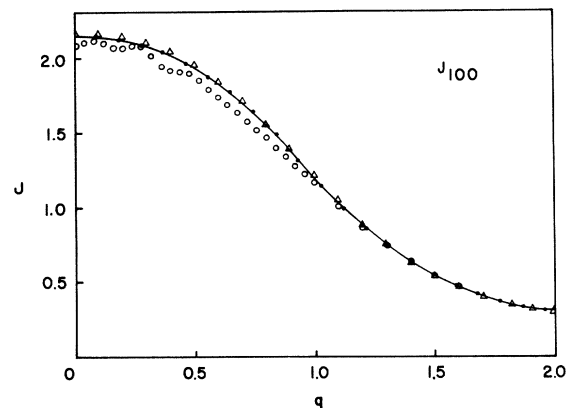


FIG. 4. Compton Profile $J(q, \hat{k})$ for $\hat{k} = (1, 0, 0)$. The open circles are the experimental results of Weiss and Phillips (Ref. 20), the triangles are the self-consistent Hartree-Fock calculations of Wepfer *et al.* (Ref. 23), and the dots connected by the solid curve are the self-consistent Hartree-Fock-Slater results of the present work. Values of q and J are given in atomic units.

Fock-Slater evaluation of ground-state properties using a contracted Gaussian basis set comprised of optimized orbitals which span the energy range of the occupied band states. The progressive relaxation of these optimized orbitals to the crystalline environment was allowed by reevaluating these optimized orbitals for each iteration and the effect of this relaxation upon the individual members of the basis set has been demonstrated. The basis so obtained combines all the advantages of a small basis set for performing accurate integrations over the Brillouin zone and the Wigner-Seitz cell, while still retaining most of the important features of a much larger basis set. Use of this basis set has permitted the economical estimation of the convergence of charge density, both with regard to multipole expansion and to the number of quadrature points used in integrating over the Brillouin zone. This investigation shows that the multipole

expansion is highly converged when truncated after the hexadecapole term ($l=4$) and that while an integration over the Brillouin zone using six points within the irreducible wedge is satisfactory for those Fourier coefficients of charge density of small wavelength, the accuracy decreases with increasing wavelength. For these long-wavelength contributions, a 19-point quadrature is employed.

The resultant self-consistent Hartree-Fock-Slater calculation predicts an indirect band gap which is in good agreement with experiment both as to its magnitude and as to the position of the minimum in the conduction band. While the self-consistent x-ray structure factors agree reasonably well with the experimental results of Göttinger and Wöfel, R factor of 3.4%, the presence of systematic trends in the residuals tends to support the conclusion of Dawson's exhaustive studies on diamond that the measurements of Göttinger and

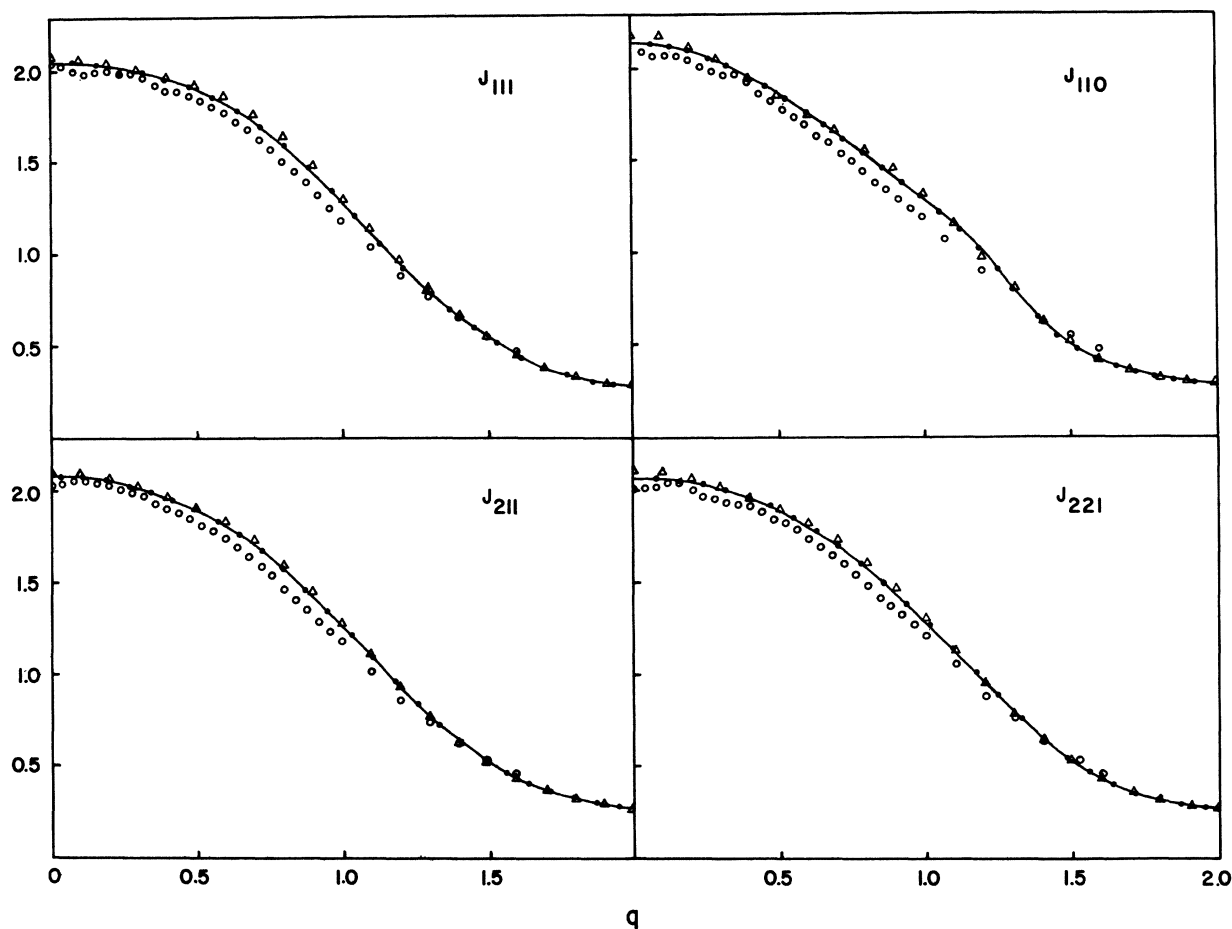


FIG. 5. Compton Profiles for lower symmetry directions. The open circles are the experimental results of Weiss and Phillips (Ref. 20), the triangles are the self-consistent Hartree-Fock calculations of Wepfer *et al.* (Ref. 23), and the dots connected by the solid curve are the self-consistent Hartree-Fock-Slater results of the present work. Values of q and J are given in atomic units.

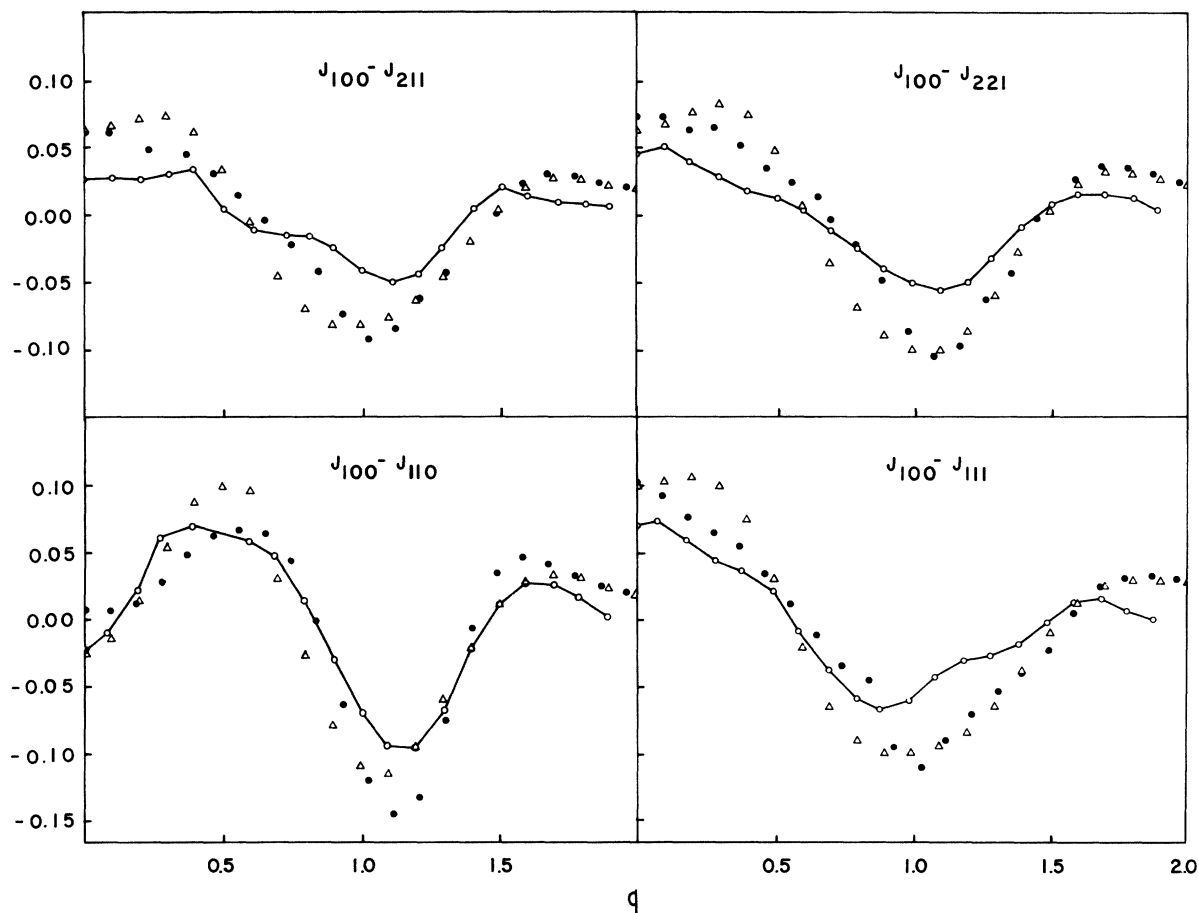


FIG. 6. Anisotropy of Compton profile. The open circles connected by solid lines are the experimental results of Reed and Eisenberger (Ref. 21), the triangles are the self-consistent Hartree-Fock calculations of Wepfer *et al.* (Ref. 23), and the solid circles are the self-consistent Hartree-Fock-Slater calculations of the present work. Values of q and J are given in atomic units.

Wöfel are not normalized to absolute intensity, but rather need to be multiplied by a scale factor somewhat greater than 1.007. Considering the unique character of diamond with its small core and strong covalent bonds, a definitive reevaluation of the experimental x-ray structure factors would be most welcome. In addition, the theoretical Compton profiles have been calculated for the five high-symmetry directions of the scattering vector for which experimental results have been reported. In all cases, the agreement with experiment is excellent. The calculated anisotropies of the Compton profile are also in excellent agreement with experiment.

Since diamond is one of the few crystalline materials for which a self-consistent Hartree-Fock calculation of band structure, x-ray scattering factors, and Compton profiles is available, it is instructive to make direct comparison of these

two different approaches. Perhaps one of the most surprising results of this investigation is that for both x-ray structure factors and Compton profiles the agreement of self-consistent Hartree-Fock-Slater with self-consistent Hartree-Fock is even better than is the agreement of Hartree-Fock-Slater with experiment. The Hartree-Fock results being in somewhat better agreement with experiment for x-ray structure factors while the situation is reversed for the Compton profiles. This agreement tends to indicate that despite the considerable conceptual differences between the local and nonlocal "exchange" operators of Hartree-Fock-Slater and Hartree-Fock, respectively, both procedures produce quantitatively similar predictions of ground-state properties when they are carried to self-consistency. This is not to imply that the two procedures are identical in all respects, since the actual band structures, for

example, differ considerably from one another.

ACKNOWLEDGMENT

This work was supported in part by Contract No. F33615-71-C-1395 issued by Aerospace Re-

search Laboratory, Air Force Systems Command, U.S. Air Force, Wright-Patterson AFB, Ohio.

The authors wish to acknowledge Dr. Chun C. Lin for his advice and helpful discussions and John Caywood for his assistance in preparation of the manuscript.

-
- ¹P. W. Kervin and E. E. Lafon, *Phys. Rev.* **58**, 1535 (1973).
- ²J. E. Simmons, C. C. Lin, D. F. Fouquet, E. E. Lafon, and R. C. Chaney, *J. Phys. C* **8**, 1549 (1975).
- ³J. R. Leite, B. I. Bennett, and F. Herman, *Phys. Rev. B* **12**, 1466 (1975).
- ⁴E. E. Lafon and C. C. Lin, *Phys. Rev.* **152**, 579 (1966).
- ⁵R. C. Chaney, T. K. Tung, C. C. Lin, and E. E. Lafon, *J. Chem. Phys.* **52**, 361 (1970).
- ⁶C. S. Wang and J. Callaway, *Phys. Rev. B* **11**, 2417 (1975).
- ⁷W. Y. Ching and C. C. Lin, *Phys. Rev. B* **14**, 620 (1976).
- ⁸R. N. Euwema, D. L. Wilhite, and G. T. Surratt, *Phys. Rev. B* **7**, 818 (1973).
- ⁹J. C. Slater, *Quantum Theory of Atomic Structure* (McGraw-Hill, New York, 1960), Vol. 2.
- ¹⁰S. Huizinga, *J. Chem. Phys.* **42**, 1293 (1965).
- ¹¹R. C. Chaney, C. C. Lin, and E. E. Lafon, *Phys. Rev. B* **3**, 459 (1971).
- ¹²R. C. Chaney, E. E. Lafon, and C. C. Lin, *Phys. Rev. B* **4**, 2734 (1971).
- ¹³C. D. Clark, P. J. Dean, and P. V. Harris, *Proc. R. Soc. Lond. A* **277**, 312 (1964).
- ¹⁴P. J. Dean, E. C. Lightowlers, and D. R. Wight, *Phys. Rev.* **140**, A352 (1965).
- ¹⁵T. Gora, R. Staley, J. D. Rimstidt, and J. Sharma, *Phys. Rev. B* **5**, 2309 (1972).
- ¹⁶F. R. McFeely, S. P. Kowalczyk, L. Ley, R. G. Lavell, R. A. Pollak, and D. A. Shirley, *Phys. Rev. B* **9**, 5268 (1974).
- ¹⁷B. Dawson, *Proc. R. Soc. Lond. A* **298**, 255 (1967).
- ¹⁸S. Göttlicher and E. Wöfel, *Z. Elektrochem.* **63**, 891 (1959).
- ¹⁹B. Dawson, *Proc. R. Soc. Lond. A* **298**, 264 (1967).
- ²⁰R. J. Weiss and W. C. Phillips, *Phys. Rev.* **176**, 900 (1968).
- ²¹W. A. Reed and P. Eisenberger, *Phys. Rev. B* **6**, 4596 (1972).
- ²²P. Eisenberger and P. M. Platzman, *Phys. Rev. A* **2**, 415 (1970).
- ²³G. G. Wepfer, R. N. Euwema, G. T. Surratt, and D. L. Wilhite, *Phys. Rev. B* **9**, 2670 (1974).